



It is not crystal clear: “nuances” in the selection of raw materials for Iron Age translucent glass revealed by chemical analyses of beads from central Italy

Oleh Yatsuk¹ · Leonie Koch² · Lorena Carla Giannossa³ · Annarosa Mangone³ · Giacomo Fiocco^{4,5} · Marco Malagodi^{4,5} · Astrik Gorghinian⁶ · Marco Ferretti⁷ · Patrizia Davit¹ · Alessandro Re⁸ · Alessandro Lo Giudice⁸ · Cristiano Iaia⁹ · Monica Gulmini¹

Received: 31 January 2024 / Accepted: 11 July 2024
© The Author(s) 2024

Abstract

The Iron Age was a period of change, with many innovations in the glass-making technology. The chemical composition of the set of objects considered in the present study demonstrates the diversity of the raw materials used and the depth of knowledge about the manipulation of glass appearance in the eighth-sixth centuries BCE. The study was carried out using fibre optics reflection spectroscopy and portable X-ray fluorescence spectrometry at the museums’ premises to examine a large number of glass beads and preliminarily group them on the basis of their composition and spectral characteristics. In addition, a smaller set of selected samples was analysed by laser ablation inductively coupled plasma mass spectrometry to provide a comprehensive chemical characterisation of the material. The compositional data indicated that the samples belonged to the high magnesium and low magnesium glass compositional types. Only one sample was recognised as low magnesium medium potassium glass. Glasses within each group were made from different sands, suggesting different provenances. Some of the samples were suggested to be of local origin, while the others were interpreted as imported glass. Evidence of glass colouring, decolouring and recycling are also discussed.

Keywords Ancient glass · Raw materials · Iron Age · pXRF · LA-ICP-MS

Introduction

One of the first steps in glass making is the selection of the raw materials. In the first half of the first millennium BCE ancient craftspeople could use silica-rich sand or crushed quartz (Moretti and Hreglich 2013; Rehren and Freestone 2015) to make the base of the glass batch, i.e. the mixture

of raw materials ready to be fused. As it was unattainable for the ancient furnaces to melt pure quartz, certain (usually alkali-rich) materials were used to obtain eutectic systems, which significantly lowered the temperature required to melt the batch (Brill 1963; Henderson 1985; Angelini et al. 2019). These materials are usually referred to as fluxing agents, or simply fluxes.

✉ Monica Gulmini
monica.gulmini@unito.it

¹ Department of Chemistry, University of Turin, Via Giuria, 7 – 10125 Turin, Italy

² Institute of Prehistoric Archaeology, University of Cologne, Weyertal 125, 50931 Cologne, Germany

³ Department of Chemistry and Laboratorio di Ricerca per la Diagnostica dei Beni Culturali, University of Bari “Aldo Moro”, Via Orabona 4, 70126 Bari, Italy

⁴ Arvedi Laboratory of Non-Invasive Diagnostics, CISRiC, University of Pavia, Via Bell’Aspa 3, 26100 Cremona, Italy

⁵ Department of Musicology and Cultural Heritage, University of Pavia, Corso Garibaldi 178, 26100 Cremona, Italy

⁶ National Institute of Nuclear Physics, National Laboratory of Frascati, Via Enrico Fermi 40, 00044 Frascati, Rome, Italy

⁷ Italian National Research Council, Institute of Heritage Science, Via Salaria Km 29.300, 00015 Montelibretti, Rome, Italy

⁸ Department of Physics, University of Turin and INFN Branch in Turin, Via Giuria, 1 - 10125 Turin, Italy

⁹ Department of Historical Studies, University of Turin, Via Sant’Ottavio, 20 – 10124 Turin, Italy

By 500 BCE, several kinds of fluxes were known: the ash of halophytic plants, the use of which resulted in the production of the so-called High Magnesium Glass (HMG); the evaporitic deposits of soda minerals, which were used for the production of the so-called Low Magnesium Glass (LMG); a material with comparable soda and potash content, which was used for the production of a specific type of mixed alkali glass (this glass was not produced during the Iron Age, though); and a potash-rich flux, which was used for the production of glass with a high potassium concentration (Shortland et al. 2006a; Moretti and Hreglich 2013; Henderson 2013; Mildner et al. 2018; Conte et al. 2018, 2019; Angelini et al. 2019; Reade 2021). The first two fluxes mentioned above were the most popular choice for glassmakers in the Mediterranean in the early first millennium BCE, but by the middle of the millennium, most of the glass circulating in the region was made by adding evaporitic minerals rich in sodium carbonates, usually referred to in the literature as natron (Shortland et al. 2006a; Panighello et al. 2012; Conte et al. 2016).

Natron glass could not be durable without the presence of a stabilising component, usually an alkali-earth oxide added in the form of lime. Several sources of lime have been hypothesised to have been used in the past, including shells and limestone, some amount of which can be present in sand (Wedepohl et al. 2011; Henderson 2013; Angelini et al. 2019). Plant ashes naturally contain certain amounts of lime, making the addition of lime to a lime-poor silica source unnecessary if plant ash is used as the fluxing agent (Tite et al. 2006; Rehren 2008).

In addition to these two or three main components, ancient artisans attempted to modify the appearance of the final product by adding colourants – usually oxides or other compounds of the transition metals (Mirti et al. 2002; Henderson 2013), and opacifiers – crystalline compounds that do not dissolve in the glass matrix, preventing light from passing through the solid (Lahlil et al. 2011; Biron and Chopinet 2013). Without the addition of these components, the glass is expected to have a light tinge related to some impurities in the silica source, which almost always contains iron minerals in different amounts. The first attempts to decolourise glass (basically, to remove the unintentional colour caused by iron) date back to the middle of the first millennium BCE (Silvestri et al. 2008; Biron and Chopinet 2013; Blomme et al. 2017; Abd-Allah 2022). The composition of glass objects has great potential to shed light on the batch formulas that have been used during times.

In order to trace the use of different raw materials during the Iron Age in the Mediterranean, a diverse set of glass objects, consisting mainly of monochrome beads and dating mainly from the eighth—seventh centuries BCE, with two objects from the sixth century BCE (out of a total of sixty-three objects) was examined in this study. They were

excavated in South Etruria and Latium (today's Lazio region of Italy). This set provides an opportunity to study the raw glass composition of finds belonging to a period still under-represented in glass studies. In fact, many of the objects discussed in this paper show no evidence of intentional addition of colouring agents and are referred to in the text as “uncoloured”. Their faint colours can be reasonably attributed to the effect of colourants (mainly iron ions) from the natural impurities of the raw materials, making it possible to establish the base glass compositional characteristic(s) and to elaborate the data in order to highlight the possible existence of several centres supplying glass to the Italian peninsula during the period under consideration.

The first part of the analytical study was carried out using non-invasive methods and portable equipment at the Museo Nazionale Etrusco di Villa Giulia and the Museo delle Civiltà (both in Rome, Italy), where the objects are kept. Fibre Optics diffuse Reflection Spectroscopy (FORS) and portable X-Ray Fluorescence spectrometry (pXRF) have been employed in this step. A smaller set of samples was then analysed in the laboratory by Laser Ablation Inductively Coupled Plasma Mass Spectrometry (LA-ICP-MS) to gain a deeper insight into the composition of the glass through a micro-invasive approach. The main aim of the pXRF survey was to highlight trends that would allow the identification of groups on a compositional basis in order to possibly extend the results obtained by LA-ICP-MS to all the samples in the same compositional group. The data set obtained by LA-ICP-MS was compared with other compositional data sets to suggest the use of specific materials and to narrow down the suggestions as to where the glass was produced.

Materials

Glass beads and other objects within the study were found in funerary contexts. They mostly belong to the inventory of the females' graves. The archaeological sites where the objects were found are located in the historical regions of South Etruria and Latium. They belong to the Early Iron Age II (800–720 BCE), Orientalising (720–580 BCE) and Archaic (580–480 BCE) periods. The sites in Etruria are the following necropolises, each pertaining to an ancient proto-urban or urban agglomeration (descriptions of the sites and graves is given in the references): Arcatelle of Tarquinia (Babbi 2003); Polledrara of Bisenzio (Delpino 1977); Vaccareccia (Palm 1952) and Quattro Fontanili of Veio (Falconi Amorelli et al. 1963); Caolino del Sasso di Furbara (Brusadin Laplace et al. 1992) and Cava della Pozzolana (unpublished) of Cerveteri; Poggio Maremma and Osteria of Vulci (Sgubini Moretti 2001); Dei Tufi necropolis of Narce (Carlucci and De Lucia 1998); Montarano of Falerii

(Ligabue 2022); Saliere (Stefaní 1912) and Monte Cornazano (Paribeni 1906) of Capena.

The Latium sites are represented by the Caracupa necropolis near Sermoneta (Mengarelli and Savignoni 1903); Riserva del Truglio near Marino (Taloni 2013) and Osteria dell'Osa necropolis, near the Roman city of Gabii, within the territory of present-day Rome (Bietti Sestieri 1992). The context for each sample is reported in Table 1. The DMS coordinates of the mentioned sites are reported in the supplementary information (Table SI 1).

All the archaeological finds considered in this study are translucent (Table 1). The majority of them – forty-nine objects – can be included into a loosely defined generic type of simple spherical and slightly oblate monochrome beads of various sizes and hues. Such beads represent the simplest idea of glass bead making, and show no clear size and colour boundaries that would allow the identification of sub-groups. In addition, their simple shape and wide distribution do not give clear archaeological evidence for period and site(s) of production, although we can consider that similar beads are well known in Italy and in the wider Mediterranean area (Reade et al. 2006; Olmeda 2015; Oikonomou and Triantafyllidis 2018; Conte et al. 2019; Koch 2020).

Other types of objects are also present in the set. Six (PG69-72, PG75 and PG76) are simple ring beads in blue, yellow and purple colours found in a single tomb (n. 48) in the necropolis of Caracupa (Sermoneta). Differently coloured ring beads (translucent and opaque) are well known in the Italian contexts (Koch 2020; Ferri et al. 2020; Yatsuk et al. 2023) though they are usually made of intensely coloured glass. Two other artefacts are the so-called bird beads of different colours (PG172 and VG88). The occurrence of these beads is frequent in Rhodes, but examples from Euboea and from Italian necropolises (around forty beads) are also known (Koch 2018). Two other finds from Vulci have a button-like appearance. They are flattened round objects with a cavity (pit) on one side with traces of iron inside, suggesting that the cavity was probably used to accommodate a metal ring for fixing them to something.

Other types include one pear-shaped object decorated with yellow waves (PG90). Its shape is reminiscent of the spindle whorls for cloth production, however the size speaks in favour of the decorative purpose of this object (used, for example, as a bead). Another find, that was recognised as the part of a fibula or a simple pin (Falconi Amorelli et al. 1963), consists of two beads of different sizes joined on a metal rod (VG56). It will be referred to as a decorative element. The list of samples also includes one so-called melon bead, featuring ribs parallel to the aperture (VG86). Such beads were produced through a long period of time in many colour variations and are widely distributed in the Mediterranean (Ignatiadou 2012; Kolesnychenko and Kiosak 2018; Kaparou and Oikonomou 2022; Yatsuk et al. 2023). Finally,

a fragment of a simple hemispherical glass bowl (VG114) was included in the list. Such bowls are rare in the Italian peninsula, but they were found more frequently in the Eastern Mediterranean, where they are thought to be produced by mould shaping (O'hea 2011; Cellerino 2021). The apparent colours of the finds are given in Table 1, and the photographs of selected representatives of the main typological group of samples, and most of the other objects, are shown in Fig. 1.

Methods

FORS

The instrumental setup consisted of a 20 W Tungsten halogen lamp HL-2000-HP-FHSA produced by Ocean Insight (Orlando, USA), a 2 m long Y-shaped fibre optic probe with a core diameter of 400 μm , and an Ocean Insight QEPro spectrometer equipped with a CCD detector (HC1 grating). The system was operated in the spectral range between 350 and 1000 nm, with an optical resolution of 6.78 nm FWHM. Before and during the analyses, the intensity of the reflected light was calibrated against a highly reflective Spectralon reference. Each spectrum was obtained as the average of at least 40 scans with a minimum dwell time of 0.019 s. During the analyses the probe was placed at an angle of approximately 45° to the surface of the object, and several spectra were acquired for each sample. As expected, some highly translucent beads did not allow spectra to be recorded in the reflectance mode. Where informative reflectance spectra were obtained, they were normalised to 100.

pXRF

Three different pXRF units were used in the museums. An XG Lab – Bruker ELIO spectrometer (XGLab S.R.L. Milan, Italy; Bruker, Billerica, MA, USA) with Rh radiation source, 25 mm² Silicon Drift Detector (SDD) was used to analyse the PG series of samples. The beam was focused on the 1.2 mm spot with the following settings: acquisition time – 90 s, current – 40 μA , voltage – 40 keV. The majority of the VG series of samples were analysed by a Unisantix XMF-104 spectrometer (Geneva, Switzerland), equipped with a Mo anode and a 7 mm² Si-PIN detector. A polycapillary optical system focused the beam on a spot of 80 μm . The following settings were used: time – 150 s, current – 300 μA and voltage – 50 keV. VG82, VG83 and VG84 were analysed by an ad-hoc instrument called Frankie, created by the Italian National Institute of Nuclear Physics-LNF (INFN-LNF Frascati, Italy). This last device has a W radiation source and a 20 mm² SDD detector. Equipped with polycapillary optics, it focuses the

Table 1 Appearance and archaeological context of the objects discussed in this study. Diameter is measured for beads as the largest dimension in the direction perpendicular to the aperture. N/A: not applicable (for bead fragments or other non-bead objects)

Inv. number	Sample name	Colour	Diameter*, mm	Site	Locality	Grave	Absolute date, years BCE	Period
Spherical-oblate monochrome beads								
25,338	PG1	Honey-yellow	16	Tarquinia	Arcatelle	-	800–720	EIAII
25,339	PG2	Honey-yellow	20	Tarquinia	Arcatelle	-	800–720	EIAII
51,946	PG7	Green	15	Bisenzio	Polledrara	Tomb 11	800–720	EIAII
51,946.001	PG8	Blue	15	Bisenzio	Polledrara	Tomb 11	800–720	EIAII
51,946.003	PG9	Blue	15	Bisenzio	Polledrara	Tomb 11	800–720	EIAII
51,946.004	PG10	Honey-yellow	12	Bisenzio	Polledrara	Tomb 11	800–720	EIAII
51,946.006	PG11	Honey-yellow	15	Bisenzio	Polledrara	Tomb 11	800–720	EIAII
51,946.01	PG12	Uncoloured	11.5	Bisenzio	Polledrara	Tomb 11	800–720	EIAII
51,946.012	PG13	Honey-yellow	N/A	Bisenzio	Polledrara	Tomb 11	800–720	EIAII
51,946.013	PG14	Honey-yellow	N/A	Bisenzio	Polledrara	Tomb 11	800–720	EIAII
51,946.014	PG15	Uncoloured	N/A	Bisenzio	Polledrara	Tomb 11	800–720	EIAII
68,026.005	PG31	Honey-yellow	5	Veio	Vaccareccia	Tomb 6	650–630	Orientalising
69,798	PG67	Honey-yellow	10.5	Sermoneta	Caracupa	Tomb 48	770–720	EIAII
69,798.004	PG68	Uncoloured	13	Sermoneta	Caracupa	Tomb 48	770–720	EIAII
87,440	PG95	Green	17	Marino	Riserva del Truglio	Tomb 3	730–600	Orientalising
87,440.001	PG96	Honey-yellow	15	Marino	Riserva del Truglio	Tomb 3	730–600	Orientalising
87,863	PG104	Honey-yellow	18	Marino	Riserva del Truglio	-	730–600	Orientalising
109,402	PG117	Honey-yellow	15	Rome	Osteria dell'Osa	Tomb 10	800–750	EIAII
109,403	PG118	Honey-yellow	N/A	Rome	Osteria dell'Osa	Tomb 10	800–750	EIAII
109,405	PG119	Uncoloured	16	Rome	Osteria dell'Osa	Tomb 10	800–750	EIAII
109,407	PG120	Honey-yellow	N/A	Rome	Osteria dell'Osa	Tomb 10	800–750	EIAII
165,945.004	PG137	Uncoloured	13	Cerveteri	Sasso di Furbara, Caolino	Tomb 29	770–730	EIAII
165,993	PG140	Honey-yellow	12	Cerveteri	Sasso di Furbara, Caolino	Tomb 34	770–730	EIAII
165,993.002	PG142	Honey-yellow	N/A	Cerveteri	Sasso di Furbara, Caolino	Tomb 34	770–730	EIAII
165,993.003	PG143	Uncoloured	N/A	Cerveteri	Sasso di Furbara, Caolino	Tomb 34	770–730	EIAII
166,019	PG145	Green	14	Cerveteri	Sasso di Furbara, Caolino	Tomb 40	770–730	EIAII
166,019	PG146	Green	14	Cerveteri	Sasso di Furbara, Caolino	Tomb 40	770–730	EIAII
166,019	PG147	Green	15	Cerveteri	Sasso di Furbara, Caolino	Tomb 40	770–730	EIAII
166,022	PG153	Honey-yellow	15	Cerveteri	Sasso di Furbara, Caolino	Tomb 40	770–730	EIAII
166,034	PG154	Honey-yellow	8	Cerveteri	Sasso di Furbara, Caolino	Tomb 41	770–730	EIAII
132,644–132,652	VG14	Honey-yellow	15	Vulci	Poggio Maremma	Tomb "a fossa profonda"	725–700	Orientalising
49,990–49997	VG48	Green	16	Cerveteri	Cava Della Pozzolana	Tomb XXVII	800–730	EIAII

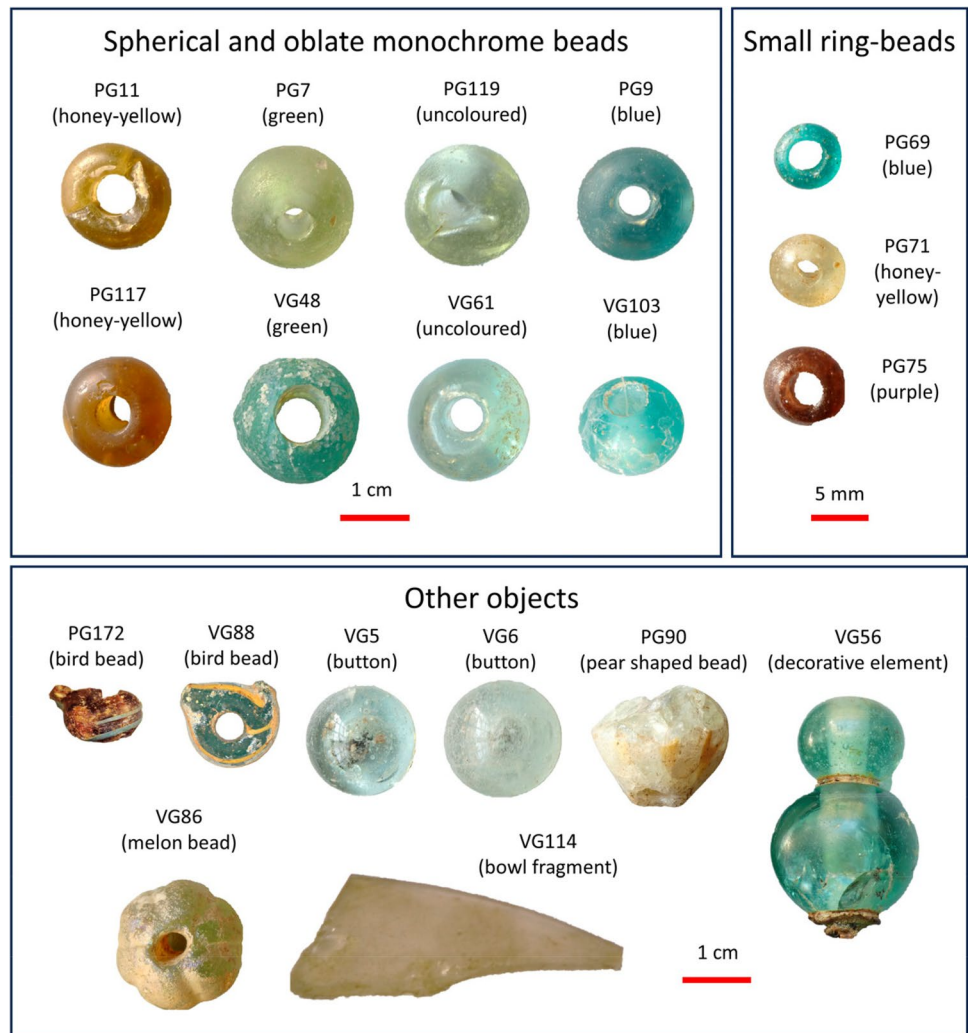
Table 1 (continued)

Inv. number	Sample name	Colour	Diameter*, mm	Site	Locality	Grave	Absolute date, years BCE	Period
49,990–49997	VG49	Green	19	Cerveteri	Cava Della Pozzolana	Tomb XXVII	800–730	EIAII
49,990–49997	VG52	Uncoloured	11	Cerveteri	Cava Della Pozzolana	Tomb XXVII	800–730	EIAII
49,990–49997	VG53	Uncoloured	14	Cerveteri	Cava Della Pozzolana	Tomb XXVII	800–730	EIAII
62,236	VG57	Green	16	Veio	Quattro Fontanili	Tomb HH 11–12	750–730	EIAII
62,236	VG61	Uncoloured	17	Veio	Quattro Fontanili	Tomb HH 11–12	750–730	EIAII
62,236	VG62	Green	12	Veio	Quattro Fontanili	Tomb HH 11–12	750–730	EIAII
62,236	VG63	Green	14	Veio	Quattro Fontanili	Tomb HH 11–12	750–730	EIAII
-	VG82	Blue	13	Narce	Necropoli dei Tufi	Tomb 1	800–720	EIAII
-	VG83	Uncoloured	18	Narce	Necropoli dei Tufi	Tomb 1	800–720	EIAII
-	VG84	Uncoloured	15.5	Narce	Necropoli dei Tufi	Tomb 1	800–720	EIAII
-	VG87	Green	14	Falerii	Montarano	Tomb 17 (XXVI)	700–600	Orientalising
-	VG89	Honey-yellow	14	Falerii	Montarano	Tomb 17 (XXVI)	700–600	Orientalising
-	VG90	Honey-yellow	13.5	Falerii	Montarano	Tomb 17 (XXVI)	700–600	Orientalising
16,530	VG102	Honey-yellow	14	Capena	Saliera	Tomb 104	800–750	EIAII
16,530	VG103	Blue	15.5	Capena	Saliera	Tomb 104	800–750	EIAII
16,530	VG104	Uncoloured	16.5	Capena	Saliera	Tomb 104	800–750	EIAII
16,530	VG105	Green	26	Capena	Saliera	Tomb 104	800–750	EIAII
Small ring-beads								
69,801.001	PG69	Blue	7	Sermoneta	Caracupa	Tomb 48	770–720	EIAII
69,801.001	PG70	Blue	7	Sermoneta	Caracupa	Tomb 48	770–720	EIAII
69,801.001	PG71	Honey-yellow	7	Sermoneta	Caracupa	Tomb 48	770–720	EIAII
69,801.001	PG72	Honey-yellow	7	Sermoneta	Caracupa	Tomb 48	770–720	EIAII
69,801.001	PG75	Purple	7	Sermoneta	Caracupa	Tomb 48	770–720	EIAII
69,801.001	PG76	Purple	6.5	Sermoneta	Caracupa	Tomb 48	770–720	EIAII
Bird beads								
109,312.005	PG172	Purple + opaque green stripe	11.5	Rome	Osteria dell'Osa	Tomb 82	750–720	EIAII
-	VG88	Green + opaque yellow stripe	12	Falerii	Montarano	Tomb 17 (XXVI)	700–600	Orientalising
Buttons								
131,433	VG5	Uncoloured	16.5	Vulci	Osteria	Kottabos tomb	520–500	Archaic
131,433	VG6	Uncoloured	17.5	Vulci	Osteria	Kottabos tomb	520–500	Archaic
Other objects								
75,266	PG90	Uncoloured body + opaque yellow wave	19	Capena	Monte Cornazzano	Tomb 100	730–675	Orientalising
66,292	VG56	Green	19	Veio	Quattro Fontanili	Tomb AA1	770–730	EIAII

Table 1 (continued)

Inv. number	Sample name	Colour	Diameter*, mm	Site	Locality	Grave	Absolute date, years BCE	Period
-	VG86	Green	21	Falerii	Montarano	Tomb 17 (XXVI)	700–600	Orientalising
-	VG114	Yellow	N/A	-	-	-	720–630	Orientalising

Fig. 1 Photographs of representative samples for each typological group (spherical, oblate and ring beads) with indication of their colour. For the other objects the type is indicated. Scale is true for all the objects in the same frame. © Museo Nazionale Etrusco di Villa Giulia and Museo delle Civiltà



X-rays into a 300 μm spot. Analysis lasted 200 s, the current was set to 80 μA , and voltage – 40 keV. Three spectra were acquired for each sample. When decorative elements of other colours were present, three additional spectra were acquired on the decoration. The procedures employed to ensure comparability between the data from the three spectrometers, and the quality of the pXRF results, are discussed with details in Yatsuk et al. (2022). Spectra were fitted using PyMCA software (Solé et al. 2007) based on the Fundamental Parameter algorithm improved by the use of matrix-matching reference materials.

LA-ICP-MS

A NexION 300 \times ICP mass spectrometer from Perkin-Elmer (Waltham, USA) coupled to an ESI NWR 213 laser ablation system (ESI New Wave Research Co., Cambridge, UK) was used. The settings, already presented in Yatsuk et al. (2023), are reported as supplementary information (Table SI 2). The laser was run for 10 s to remove the first (possibly altered) surface, in order to allow the sampling of pristine material for the mass spectrometric analysis. The signal from 38 masses was measured. As discussed with details in a

previous paper (Yatsuk et al. 2023), accuracy was estimated based on data for CMOG A and NIST 614 reference glasses, which were used for quality control throughout the analyses, and it is reported as supplementary information (Table SI 3). The final composition of the sample was determined as the average of three to five acquisitions. The Ca concentration obtained from the pXRF analyses were used as the internal standard. The data were normalised to 100% after converting the elemental concentrations of the major and minor elements to their respective oxides.

Results

FORS

Diffuse reflectance did not allow to record meaningful spectra for all the samples considered, and only samples that produced meaningful spectral information are included in this section. Most of the beads can be considered as different varieties of “aqua” colour, whereas other samples show more intense hues. Glasses of different shades yielded different spectra (Fig. 2), supporting the detection of the colouring species (Mirti et al. 2002; Micheletti et al. 2020). The spectra of the honey-yellow samples are characterised by the

intense absorption in the UV-blue region of the spectrum (350–500 nm), where absorption bands of Fe^{3+} can be distinguished (Fig. 2a). Absorptions in the range 480–520 nm can be caused by Mn^{3+} ions, which are not expected to contribute any yellow colour to glass. Further insight into the presence of manganese will be given in the subsequent sub-sections of the results, where data from pXRF and LA-ICP-MS are reported. The NIR part of the spectra is highly variable in the relative reflectance, mainly due to the presence of Fe^{2+} ions in variable concentration. The small ring-beads of yellow colour (PG71, PG72) yielded a different kind of spectrum, with extremely intense UV-blue and no NIR absorption (Fig. 2a).

Blue samples are, expectedly, reflecting more light in the blue region (Fig. 2b), but this was obtained by different chemical species. Most of the blue samples have intense Fe^{2+} absorption in the NIR region, whereas small ring-beads show different spectra: the blue ones (PG69 and PG70) have their maximum of reflectance shifted towards the green region, at the same time the maximum absorption is registered at 750–900 nm, which corresponds to the absorption band of Cu^{2+} .

The purple samples (PG75 and PG76) show even more shifted reflectance maxima (around 600 nm) and a Mn^{3+} band centred at 490 nm (Fig. 2b).

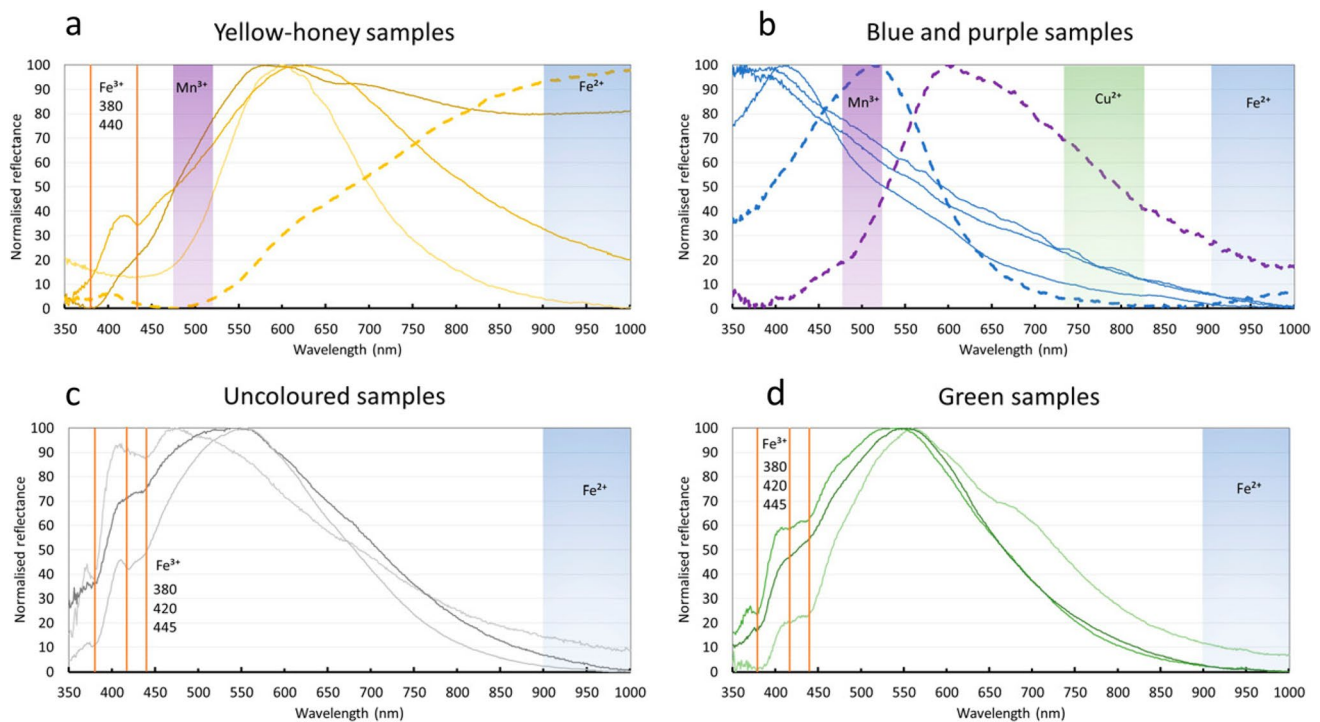


Fig. 2 Examples of FORS spectra of different coloured samples: a – honey-yellow samples. The dotted line indicates the spectrum of PG71 (small ring bead); b – blue and purple samples. The spectra of small ring beads PG69 (blue) and PG75 (purple) are given as dot-

ted lines; c – uncoloured samples; d – green samples. Fe^{3+} bands are marked with vertical lines; Mn^{3+} , Cu^{2+} and Fe^{2+} bands are marked as wavelength ranges. A summary of the absorption bands for dissolved ions in glass is given by Micheletti et al. (2020)

Samples with very weak colouration (termed as uncoloured throughout the text) show pronounced Fe^{3+} and Fe^{2+} bands (Fig. 2c), with no Mn^{3+} detected. Spectra for samples with green colouration (Fig. 2d) are not significantly different from those of the uncoloured samples, suggesting iron ions as the main colouring agents. The lower reflectance in the yellow–red region of the spectrum (600–700 nm) suggests a higher contribution of Fe^{2+} with respect to Fe^{3+} to the final colour of the glass.

It is worth noting that in some samples, the spectrum shows a band centred around 650 nm (Fig. 2a and d), the origin of which is unclear.

pXRF

The results of the pXRF measurements are reported as supplementary information (Table SI 4). As discussed in Yatsuk et al. (2022), the accuracy of the pXRF data may not be ideal for some elements, but the data set still had the advantage of allowing compositional groups to be highlighted. In all the typological groups of samples, only Ca, Fe, and Sr are always present above the quantification limits of the pXRF instruments. Nevertheless, the non-invasive screening allowed some preliminary inspection of the compositional features of the samples. K_2O is above 1% (note that the limit of quantification for the ELIO pXRF unit is 1.2%) in all the green spherical and oblate beads; elevated concentrations were also recorded in about half of the uncoloured beads and in a few of the blue and yellow beads. This suggests that 1% K_2O can be set as a preliminary threshold to distinguish compositional groups of samples. By comparing the two groups of spherical and oblate monochrome beads (the “low K_2O ” and the “high K_2O ”, with concentrations of K_2O above and below 1% respectively), other compositional

differences can be observed (Fig. 3). Although the groups are not perfectly resolved, it is evident that the high K_2O samples tend to have a lower CaO/SrO ratio (median value 161, st.dev. 23) compared to the low K_2O samples (median 196, st. dev. 29). Some samples in the low K_2O group have a lower CaO/SrO ratio, suggesting that these samples were not assigned to the high K_2O group because of their K_2O content was slightly below 1%, which is below the limit of quantification of the ELIO pXRF unit. Samples PG104 and VG83 gave extremely high values for CaO/SrO (94 and 760 respectively) and are not included in Fig. 3.

In addition, the high K_2O samples tend to have a higher amount of Fe_2O_3 (0.58% on average) compared to the low K_2O beads (0.32% on average). Consequently, the former group has a higher $\text{Fe}_2\text{O}_3/\text{SrO}$ ratio than the latter. The same samples in the low K_2O group that have a CaO/SrO ratio similar to that of the high K_2O group (namely, PG118, PG154 and VG52) also have a similar $\text{Fe}_2\text{O}_3/\text{SrO}$ ratio, confirming that they can be included in the high K_2O group.

With regard to the other typological groups, the small ring beads and the bird beads are strongly associated with the other high K_2O beads (Fig. 3), although in some of them the K_2O concentration was below the quantification limit. The other objects, with the exception of PG90, all have their K_2O concentrations above 1%. Finally, the buttons seem to stand out from this general picture, as they have different K_2O levels that would not allow them to be assigned to one of the two main compositional groups in terms of oxide ratios.

Transition metals were sporadically detected at concentrations above 0.1%. MnO was detected in all purple glasses, which (together with the evidence from FORS) indicates its use for colouring. Noteworthy is its presence in some uncoloured and honey-yellow samples (PG2, PG104, VG53,

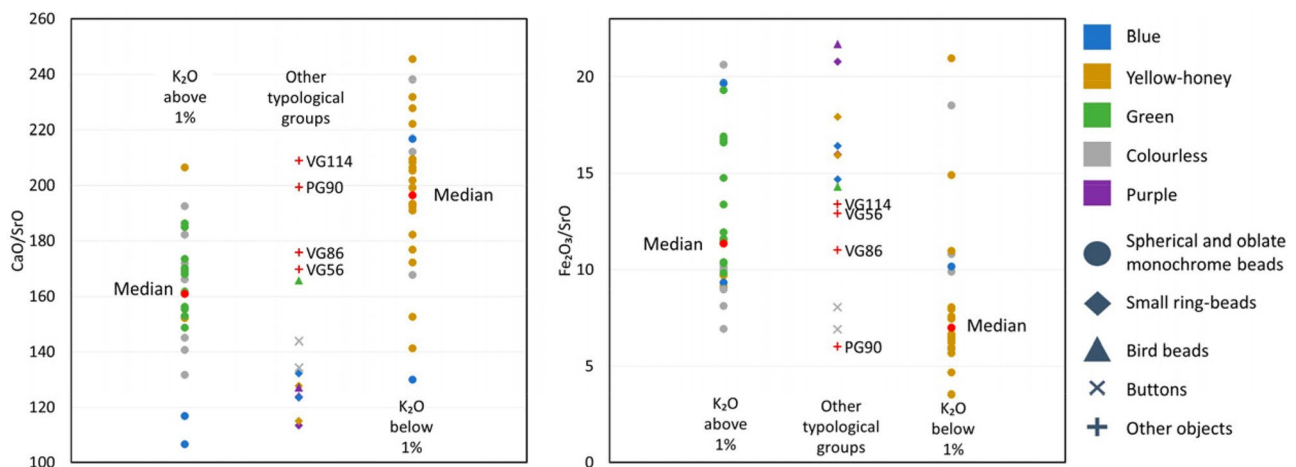


Fig. 3 Ratio of CaO and Fe_2O_3 to SrO (pXRF data). Markers, one for each typological group, are coloured according to the colour of the samples. Outliers (PG104 and VG83) are not reported in the plots

VG61, VG104) and one green sample (PG147). Copper is a green–blue colourant, and it was indeed detected in some blue and green samples (PG69, PG70, VG57, VG63, VG82, VG88, VG103), but also in uncoloured (VG52, VG83) and yellow (VG102, VG114) samples. Copper was probably also used to colour the decorative glass on the bird bead PG172. Another bird bead decoration (VG88) was probably coloured by lead antimonate, based on the detection of the elevated PbO and Sb₂O₅ concentrations in the decorative element compared to the bulk of the bead. Antimony (without associated lead) was detected in many green and uncoloured samples at concentration mainly below 1% by weight as oxide.

LA-ICP-MS

Twenty samples were allowed to reach the laboratory for LA-ICP-MS analysis. These data will form the basis of the discussion on raw materials and will integrate the pXRF data to extend the interpretation of the elemental evidence to the wider set of the samples.

The major and minor element compositions determined by LA-ICP-MS (expressed as oxides) are presented in Table 2. The data for major elements allow all the samples to be assigned to soda-lime-silica glass. However, the variability of other major oxides, such as MgO and Al₂O₃ suggests the use of different raw materials. Iron is consistently present in minor quantities (usually less than 1% oxide by weight). MnO and Sb₂O₅ concentrations are elevated in a number of samples, as already suggested by the pXRF data. The other oxides listed in Table 2 are present at near trace concentrations (below 1000 ppm). The yellow decoration of PG90 is probably coloured by lead antimonate, as indicated by the elevated concentrations of lead and antimony in the decorative element compared to the bulk of the bead.

The concentrations of trace elements determined by the LA-ICP-MS are given in Table 3. The data show some variability for Sr, Ba and Ce, which will be discussed in the following section.

Discussion

Both pXRF and LA-ICP-MS results allow to distinguish two compositional groups divided by their K₂O concentrations. LA-ICP-MS analyses showed that the group with the higher K₂O concentration (above 0.5%) also contains at least 2% by weight of MgO. In the literature, such glasses are usually referred to as HMG, with Egyptian examples for LBA and IA glass featuring the lowest concentration of K₂O (Sayre and Smith 1961; Rehren 2000; Mirti et al. 2008; Purowski et al. 2018; Angelini et al. 2019; Conte et al. 2019). For these samples, no correlation emerged between the concentration of MgO and that of lime or other silica-related

oxides, further supporting the hypothesis that the glass was prepared with plant ash. Samples with high Na₂O concentrations and both MgO and K₂O concentrations below 0.5% can be attributed to natron (LMG) glass production (Sayre and Smith 1961; Henderson 1985; Shortland et al. 2006a; Conte et al. 2019). The concentration of other elements further supports the existence of two compositional groups, as shown in Fig. 4, which shows the CaO/SrO vs Fe₂O₃/SrO binary plots obtained for both the pXRF and the LA-ICP-MS datasets. It can be seen that the high K₂O (HMG) and low K₂O (LMG) samples tend to cluster in different areas of the plots showing some consistency, although the division between the groups is not very clear. PG118, PG154 and VG52, that are assigned to the low K₂O group by the pXRF data, are instead grouped with the high K₂O group by the LA-ICP-MS data. On the other hand, PG2 and VG61 were attributed to the high K₂O group, but are in the low K₂O group (pXRF data). It can be assumed with reasonable confidence that all the small ring beads, bird beads and most of the other objects (VG56, VG86, VG114) can be assigned to the HMG group. The glass buttons, on the other hand, remain undetermined in this classification, although they seem to be closer to the LMG samples.

No evident chronological division emerge between these compositional groups. Moreover, the present sample set of translucent glass from South Etruria and Latium is approximately equally subdivided between HMG and LMG glass (thirty-four HMG samples against twenty-seven LMG samples based on the pXRF data).

The composition of PG104 makes this sample an outlier: its concentration of Al₂O₃, and the amount of some major oxides and transition metals, are more similar to the so-called LMMK glasses (Low Magnesium Medium Potassium), for which the use of evaporitic deposits has been proposed (Purowski et al. 2012).

Some information about the provenance of the raw glass can be obtained by the content of the elements that are associated with the silica source, as it is assumed that the chemical composition of the silica source used in glassmaking can be reflected to some extent in the composition of the base glass (Brems and Degryse 2014). We therefore compared the minor and trace element content of the samples considered here with each other and with other coeval glasses for which a region of provenance has been suggested.

As far as TiO₂ and Fe₂O₃ concentrations are concerned, they are strongly correlated with each other throughout the dataset (except for PG104, which is an outlier), with a correlation coefficient of 0.7. However, if the established HMG and LMG compositional groups are considered separately, the correlation coefficient rises even higher (0.93 and 0.9 respectively). The TiO₂/Fe₂O₃ ratio is also different between the groups: 0.12 (st. dev. 0.02) and 0.22 (st. dev. 0.07) for HMG samples and LMG samples, respectively. This could

Table 2 LA-ICP-MS results. Compositions of the analysed samples (major and minor oxides in weight percent). “y” after the name of PG90 means yellow part

Sample/st.dev	Na ₂ O	MgO	Al ₂ O ₃	SiO ₂	K ₂ O	CaO	TiO ₂	V ₂ O ₅	MnO	Fe ₂ O ₃	CoO	NiO	CuO	ZnO	As ₂ O ₃	SnO ₂	Sb ₂ O ₃	PbO	
Spherical and oblate monochrome beads																			
PG2	17	2.5	0.34	70	0.9	7	0.030	0.0015	0.25	0.22	0.0002	0.0009	0.0018	0.0035	0.0005	0.0042	0.20	0.0011	
<i>st.dev</i>	3	0.4	0.05	10	0.1	1	0.005	0.0002	0.04	0.04	0.0001	0.0002	0.0006	0.0007	0.0001	0.0033	0.04	0.0005	
PG7	14.4	2.5	0.77	72	0.81	7.0	0.054	0.0018	0.023	0.48	0.0003	0.0013	0.0007	0.0032	0.0009	0.00001	0.69	0.0005	
<i>st.dev</i>	0.4	0.1	0.03	3	0.02	0.3	0.002	0.0001	0.001	0.02	0.00001	0.00001	0.0002	0.0002	0.0001	0.00003	0.08	0.0002	
PG9	16	3	1.0	70	1.3	8	0.04	0.0016	0.04	0.4	0.0037	0.005	0.0007	0.006	0.0015	0.0001	0.0008	0.0005	
<i>st.dev</i>	6	1	0.3	22	0.4	3	0.01	0.0005	0.01	0.1	0.0012	0.002	0.0001	0.002	0.0004	0.00001	0.0002	0.0001	
PG10	15	0.8	0.21	80	0.4	6	0.022	0.0005	0.006	0.12	0.0001	0.0001	0.0006	0.0009	0.0001	0.00001	0.0005	0.0002	
<i>st.dev</i>	3	0.2	0.04	10	0.1	1	0.004	0.0001	0.001	0.03	0.0001	0.0001	0.0001	0.0002	0.0001	0.00001	0.0001	0.0001	
PG13	19.3	0.41	0.15	74	0.22	5.92	0.016	0.0005	0.004	0.11	0.0001	0.0001	0.002	0.0006	0.0006	0.00001	0.0005	0.0004	
<i>st.dev</i>	0.3	0.01	0.01	1	0.01	0.03	0.000	0.00001	0.001	0.01	0.0001	0.0001	0.001	0.0001	0.0001	0.00001	0.0001	0.0002	
PG14	20	0.5	0.19	70	0.31	7	0.025	0.0006	0.005	0.14	0.0001	0.0002	0.02	0.0011	0.0003	0.0001	0.0006	0.003	
<i>st.dev</i>	4	0.1	0.05	20	0.09	2	0.006	0.0002	0.002	0.05	0.0001	0.0001	0.01	0.0007	0.0001	0.0001	0.0005	0.001	
PG15	18	0.54	0.25	75	0.24	5.1	0.055	0.0008	0.008	0.19	0.0001	0.0002	0.0011	0.0012	0.0004	0.00001	0.0007	0.0001	
<i>st.dev</i>	1	0.03	0.01	61	0.02	0.3	0.004	0.0001	0.001	0.02	0.0001	0.0001	0.0003	0.0001	0.0001	0.00001	0.0001	0.0001	
PG68	19	2.1	0.52	68	0.58	9.6	0.051	0.0012	0.016	0.35	0.0002	0.0007	0.0024	0.005	0.0002	0.0005	0.00001	0.002	
<i>st.dev</i>	1	0.1	0.04	5	0.02	0.5	0.004	0.0001	0.001	0.03	0.0001	0.0004	0.0008	0.002	0.0001	0.0008	0.00001	0.0001	
PG96	19	0.45	0.18	73	0.27	6.7	0.022	0.0006	0.004	0.12	0.0001	0.0001	0.0009	0.0006	0.0001	0.00001	0.0001	0.0012	
<i>st.dev</i>	2	0.04	0.01	6	0.02	0.5	0.002	0.00001	0.001	0.01	0.0001	0.0001	0.0009	0.0001	0.0001	0.00001	0.0001	0.0001	
PG104	29	1.3	10	50	1.5	2.8	0.8	0.012	1.1	4	0.004	0.0025	0.005	0.006	0.011	0.0003	0.0001	0.0014	
<i>st.dev</i>	9	0.4	3	20	0.5	0.9	0.3	0.004	0.3	1	0.001	0.0007	0.002	0.002	0.003	0.0001	0.0001	0.0004	
PG118	11	0.5	0.37	80	0.21	7	0.08	0.0012	0.009	0.27	0.0001	0.0003	0.0014	0.0009	0.0005	0.00001	0.0001	0.0005	
<i>st.dev</i>	8	0.1	0.07	20	0.06	1	0.02	0.0002	0.002	0.04	0.0001	0.0001	0.0003	0.0001	0.0001	0.00001	0.0001	0.0001	
PG119	20	3.0	0.65	66	0.82	7.8	0.056	0.0020	0.042	0.51	0.0003	0.0012	0.0018	0.0033	0.0015	0.0004	0.50	0.0008	
<i>st.dev</i>	1	0.2	0.03	6	0.06	0.5	0.004	0.0001	0.003	0.03	0.0001	0.0001	0.0002	0.0002	0.0001	0.0005	0.02	0.0004	
PG137	18	0.31	0.12	80	0.22	6	0.016	0.0005	0.003	0.10	0.0001	0.0001	0.02	0.003	0.0006	0.001	0.001	0.002	
<i>st.dev</i>	3	0.06	0.02	10	0.03	1	0.003	0.0001	0.001	0.03	0.0001	0.0001	0.03	0.003	0.0003	0.002	0.001	0.002	
PG142	21	0.35	0.15	72	0.18	6.6	0.038	0.0006	0.005	0.11	0.0001	0.0001	0.003	0.0006	0.0005	0.00001	0.00001	0.0001	
<i>st.dev</i>	3	0.05	0.02	9	0.02	0.9	0.005	0.0001	0.001	0.01	0.0001	0.0001	0.002	0.0001	0.0001	0.00001	0.00001	0.0001	
PG143	19	0.7	0.3	70	0.3	5	0.04	0.0009	0.009	0.23	0.0001	0.0002	0.0018	0.0013	0.0005	0.0001	0.00001	0.0016	
<i>st.dev</i>	7	0.2	0.1	20	0.1	2	0.01	0.0003	0.003	0.09	0.0001	0.0001	0.0005	0.0005	0.0002	0.0001	0.00001	0.0006	
PG147	17	4.7	0.47	70	2.0	8	0.040	0.0013	0.026	0.38	0.0002	0.0011	0.0008	0.0039	0.0012	0.0001	0.30	0.0005	
<i>st.dev</i>	3	0.7	0.07	10	0.3	1	0.006	0.0002	0.004	0.06	0.0001	0.0002	0.0002	0.0006	0.0002	0.0001	0.04	0.0001	
Small ring-beads																			
PG71	17	3.3	0.8	70	0.6	9	0.07	0.0023	0.12	0.6	0.0003	0.0013	0.004	0.0030	0.0003	0.0001	0.0008	0.0003	
<i>st.dev</i>	4	0.8	0.2	20	0.2	2	0.02	0.0006	0.03	0.2	0.0001	0.0004	0.001	0.0009	0.0002	0.0001	0.0003	0.0001	

Table 2 (continued)

Sample/st.dev	Na ₂ O	MgO	Al ₂ O ₃	SiO ₂	K ₂ O	CaO	TiO ₂	V ₂ O ₅	MnO	Fe ₂ O ₃	CoO	NiO	CuO	ZnO	As ₂ O ₃	SnO ₂	Sb ₂ O ₃	PbO	
PG75	16	3.0	0.88	66	0.60	9.1	0.068	0.0047	1.9	0.60	0.0006	0.0018	0.009	0.0040	0.0003	0.0001	0.0006	0.0003	
<i>st.dev</i>	<i>1</i>	<i>0.1</i>	<i>0.04</i>	<i>3</i>	<i>0.03</i>	<i>0.3</i>	<i>0.003</i>	<i>0.0002</i>	<i>0.1</i>	<i>0.03</i>	<i>0.0001</i>	<i>0.0001</i>	<i>0.001</i>	<i>0.0003</i>	<i>0.0001</i>	<i>0.0001</i>	<i>0.0001</i>	<i>0.0001</i>	
Other objects																			
PG90	15	0.57	0.33	68.34	0.09	11.22	0.061	0.0009	0.010	0.24	0.0001	0.0002	0.002	0.0013	0.0015	0.004	3.8	0.0035	
<i>st.dev</i>	<i>5</i>	<i>0.07</i>	<i>0.04</i>	<i>6.31</i>	<i>0.01</i>	<i>1.28</i>	<i>0.006</i>	<i>0.0001</i>	<i>0.001</i>	<i>0.02</i>	<i>0.0001</i>	<i>0.0001</i>	<i>0.001</i>	<i>0.0005</i>	<i>0.0002</i>	<i>0.003</i>	<i>0.3</i>	<i>0.0008</i>	
PG90y	2	0.5	0.4	73.95	0.06	7.52	0.067	0.0025	0.010	0.8	0.0002	0.0007	0.006	0.003	0.04	0.002	2.1	12.2693	
<i>st.dev</i>	<i>1</i>	<i>0.2</i>	<i>0.2</i>	<i>31.95</i>	<i>0.03</i>	<i>3.44</i>	<i>0.029</i>	<i>0.0002</i>	<i>0.005</i>	<i>0.3</i>	<i>0.0001</i>	<i>0.0004</i>	<i>0.002</i>	<i>0.001</i>	<i>0.02</i>	<i>0.001</i>	<i>0.9</i>	<i>5.6828</i>	
VG114	17	5	0.7	65.52	1.76	8.43	0.055	0.0018	0.015	0.4	0.0002	0.0013	0.0007	0.006	0.0004	0.00001	0.39	0.0003	
<i>st.dev</i>	<i>4</i>	<i>1</i>	<i>0.2</i>	<i>16.68</i>	<i>0.44</i>	<i>2.05</i>	<i>0.014</i>	<i>0.0005</i>	<i>0.004</i>	<i>0.1</i>	<i>0.0001</i>	<i>0.0003</i>	<i>0.0002</i>	<i>0.001</i>	<i>0.0002</i>	<i>0.00001</i>	<i>0.09</i>	<i>0.0001</i>	

be evidence of the use of different sands to produce these glasses, and consequently of different origins of the glass, since both titanium and iron are almost exclusively associated with the impurities in the silica source in the quantities observed here (Degryse 2014).

Looking at the UCC-normalised profile of the trace elements (Fig. 5) it can be seen that the HMG samples tend to have positive Ba and Ce anomalies (Fig. 5a), while the LMG samples have a positive Hf anomaly (Fig. 5b). Besides this general indication, it is important to stress that there is a certain heterogeneity within each group. In the HMG group, samples PG2, PG68 and VG114 have a weaker Ba anomaly, and none at all for Ce values. They also have a slightly higher TiO₂/Fe₂O₃ ratio, which brings them closer to the LMG samples.

VG114 is the only piece of a vessel within the samples investigated here, and its typological attribution and composition place it in close association with similar bowls from Gordion and Nimrud (Reade et al. 2009), thus suggesting a separate site of origin for the raw glass of this bowl.

The LMG group also shows some variability, with samples with high Hf values and others with relatively flat trace element profiles, such as PG10, PG13, PG14, PG96 and PG137. The profile of sample PG14 is shown in Fig. 5b for comparison with PG90, which shows a significant enrichment in REE, and even more so in Hf. These trends suggest that the LMG glass in this study may originate from two separate silica sources: one rich in REE and zircon (containing Zr and Hf bearing minerals) and another with lower impurity levels.

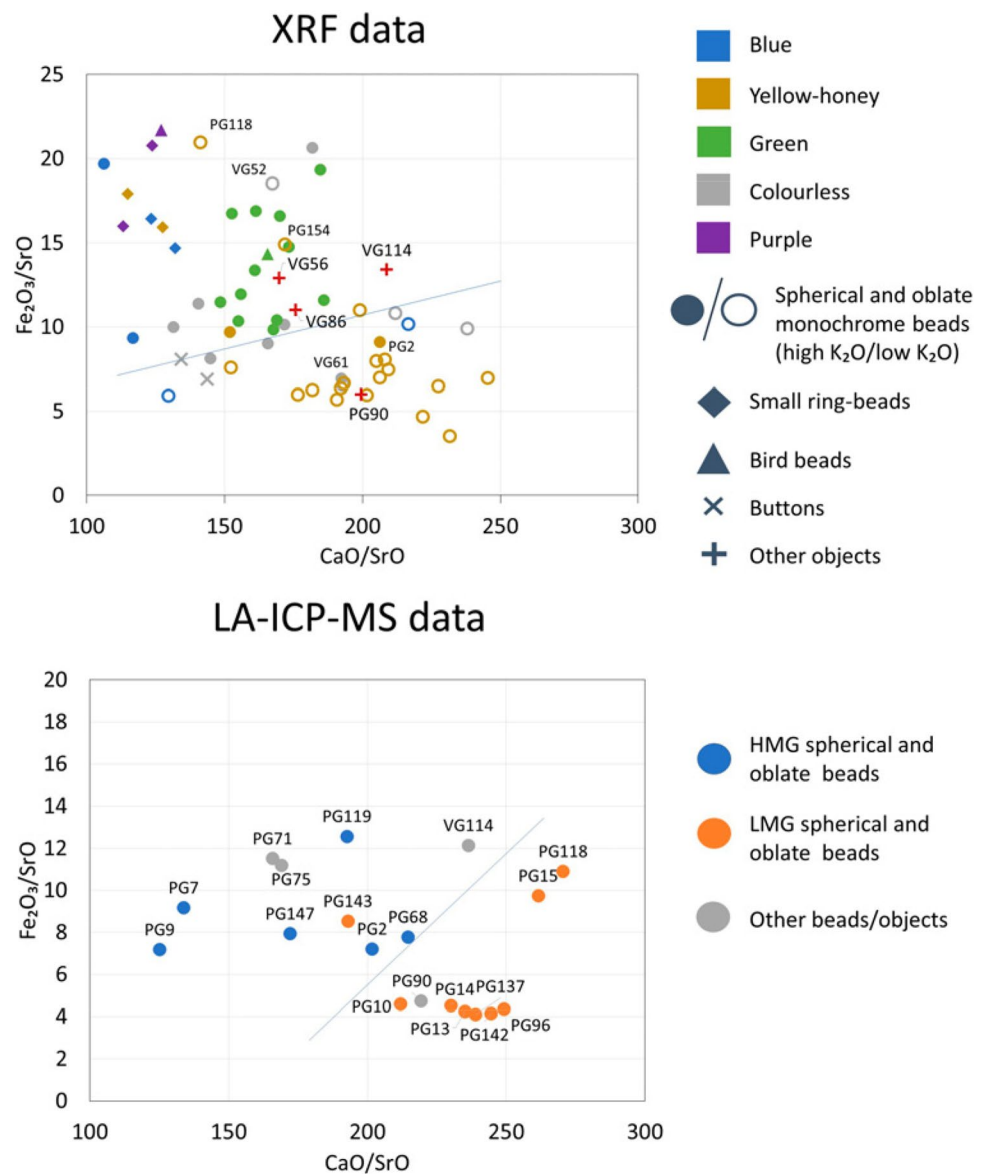
The high-Hf glasses are usually associated with Egypt, where sands have an elevated zircon content (Shortland et al. 2007). Furthermore, they show compositional parallels with other glasses found in Italy and the Eastern Mediterranean (Blomme et al. 2017; Conte et al. 2019; Reade 2021; Costa et al. 2021; Yatsuk et al. 2023). Samples with a flat trace element profile do not have pronounced compositional features that would facilitate the search for their origin, but such glasses have been found elsewhere in Italy (Conte et al. 2019). Samples with high relative Ba and Ce concentrations are only similar to a handful of samples from Southern Italy (Francavilla Marittima) presented in Conte et al. (2019). For these samples, a local production can be suggested, since (to the best of the authors' knowledge) there are no glasses with a similar trace element profile outside of the Italian peninsula.

Unfortunately, the (rare) bird beads associated with HMG by pXRF could not be analysed in the laboratory with LA-ICP-MS, so their trace element profiles are not yet available. This is an important point that deserves further research: if the bird beads have similar Ba and Ce concentrations to the samples from Francavilla Marittima samples, then they may have been produced locally, which

Table 3 LA-ICP-MS results. Trace elements concentrations of the analysed samples expressed in ppm. <LOQ – below the limit of quantification, N/A – not analysed. “y” after the name of PG90 means yellow part

Sample Id	Rb	Sr	Zr	Cs	Ba	La	Ce	Nd	Sm	Eu	Gd	Tb	Dy	Er	Yb	Lu	Hf	Tl	Th	U
Spherical and oblate monochrome beads																				
PG2	5.2	260	<LOQ	0.17	46	1.3	3.1	1.2	0.26	0.06	0.23	0.03	0.23	0.12	0.10	0.02	0.28	0.01	0.33	1.7
<i>st.dev</i>	0.8	40	-	0.03	8	0.2	0.6	0.1	0.09	0.03	0.05	0.01	0.04	0.02	0.02	0.01	0.03	0.01	0.08	0.3
PG7	5.67	440	<LOQ	0.15	67	3.3	26	3.09	0.61	0.12	0.55	0.08	0.47	0.26	0.25	0.03	0.50	0.001	0.58	0.73
<i>st.dev</i>	0.08	20	-	0.03	3	0.1	1	0.08	0.05	0.01	0.04	0.01	0.06	0.01	0.03	0.01	0.04	0.002	0.03	0.06
PG9	3	500	<LOQ	0.08	100	4	16	4	0.8	0.21	0.8	0.09	0.6	0.3	0.3	0.05	0.4	<LOQ	0.6	0.9
<i>st.dev</i>	1	200	-	0.03	30	1	5	1	0.3	0.06	0.4	0.03	0.2	0.1	0.1	0.02	0.1	-	0.2	0.3
PG10	3.2	230	<LOQ	0.07	60	1.0	1.9	0.9	0.17	0.04	0.18	0.02	0.20	0.11	0.12	0.02	0.34	0.003	0.25	0.24
<i>st.dev</i>	0.6	40	-	0.02	10	0.2	0.4	0.1	0.05	0.01	0.05	0.01	0.04	0.04	0.03	0.01	0.07	0.002	0.06	0.06
PG13	1.78	213	6.4	0.05	43.6	0.79	1.39	0.74	0.20	0.05	0.23	0.02	0.16	0.13	0.11	0.01	0.13	0.003	0.17	0.39
<i>st.dev</i>	0.04	2	0.1	0.01	0.8	0.01	0.04	0.05	0.08	0.01	0.05	0.01	0.03	0.03	0.01	0.001	0.02	0.005	0.04	0.04
PG14	3	260	17	0.08	50	1.1	1.8	0.9	0.3	0.03	0.15	0.03	0.18	0.10	0.14	0.02	0.4	0.003	0.18	0.3
<i>st.dev</i>	1	70	4	0.04	10	0.3	0.5	0.3	0.1	0.01	0.08	0.01	0.09	0.06	0.04	0.01	0.1	0.011	0.01	0.1
PG15	3.1	170	61	0.09	26	3.4	5.2	3.1	0.6	0.13	0.6	0.09	0.45	0.29	0.30	0.05	1.4	<LOQ	0.51	0.46
<i>st.dev</i>	0.2	10	4	0.01	2	0.2	0.4	0.1	0.1	0.01	0.1	0.02	0.06	0.06	0.10	0.01	0.2	-	0.07	0.07
PG68	4.4	380	N/A	0.12	76	2.2	4.2	2.0	0.45	0.11	0.45	0.06	0.44	0.28	0.26	0.04	0.56	0.01	0.44	0.40
<i>st.dev</i>	0.8	30	N/A	0.08	6	0.2	0.2	0.2	0.04	0.02	0.02	0.01	0.05	0.04	0.03	0.01	0.06	0.01	0.07	0.04
PG96	2.0	230	12.9	0.06	44	0.79	1.4	0.70	0.24	0.03	0.13	0.02	0.16	0.13	0.08	0.02	0.27	0.001	0.17	0.20
<i>st.dev</i>	0.1	20	0.7	0.01	4	0.06	0.1	0.01	0.05	0.01	0.04	0.01	0.02	0.06	0.03	0.01	0.06	0.002	0.01	0.04
PG104	60	200	N/A	1.7	700	24	50	23	5	1.05	5	0.7	5	3	3	0.51	7	0.07	7	3
<i>st.dev</i>	20	60	N/A	0.5	200	8	20	7	2	0.33	2	0.2	2	1	1	0.15	2	0.02	2	1
PG118	2.1	200	100	0.07	32	4.2	7	3.7	0.8	0.15	0.7	0.10	0.6	0.42	0.43	0.06	2.3	0.005	0.7	0.7
<i>st.dev</i>	0.4	40	20	0.02	6	0.7	1	0.8	0.1	0.01	0.2	0.04	0.1	0.09	0.09	0.01	0.4	0.003	0.1	0.1
PG119	5.0	300	N/A	0.09	61	3.1	17	3.1	0.62	0.14	0.61	0.07	0.34	0.22	0.25	0.03	0.34	<LOQ	0.38	0.74
<i>st.dev</i>	0.2	20	N/A	0.02	3	0.1	1	0.2	0.05	0.03	0.07	0.01	0.05	0.02	0.03	0.01	0.03	-	0.05	0.07
PG137	3.67	200	7	0.10	51	0.7	1.6	0.7	0.13	0.05	0.22	0.02	0.14	0.10	0.11	0.01	0.16	0.03	0.11	0.2
<i>st.dev</i>	0.4	1	0.08	9	0.2	0.9	0.2	0.04	0.04	0.07	0.01	0.02	0.02	0.03	0.01	0.07	0.03	0.03	0.04	0.1
PG142	1.8	230	51	0.07	34	1.7	2.8	1.5	0.31	0.07	0.33	0.05	0.27	0.16	0.19	0.03	1.1	0.001	0.29	0.8
<i>st.dev</i>	0.2	30	7	0.02	5	0.3	0.6	0.1	0.08	0.01	0.04	0.01	0.05	0.04	0.02	0.01	0.2	0.004	0.03	0.2
PG143	4	230	30	0.10	40	2.0	4	1.8	0.4	0.07	0.4	0.07	0.4	0.20	0.2	0.04	0.7	<LOQ	0.4	2.2
<i>st.dev</i>	1	80	10	0.05	10	0.8	1	0.7	0.3	0.05	0.1	0.04	0.1	0.08	0.1	0.02	0.3	-	0.2	0.9
PG147	8	400	<LOQ	0.10	62	2.5	9	2.4	0.50	0.10	0.44	0.06	0.34	0.21	0.18	0.03	0.37	0.001	0.43	1.1
<i>st.dev</i>	1	60	-	0.02	9	0.4	1	0.4	0.04	0.01	0.02	0.01	0.06	0.03	0.04	0.01	0.08	0.001	0.06	0.2
Small ring-beads																				
PG71	3.6	500	N/A	0.07	230	2.71	11	2.7	0.6	0.13	0.5	0.07	0.5	0.25	0.21	0.03	0.40	0.002	0.4	0.5
<i>st.dev</i>	0.9	100	N/A	0.02	50	0.75	3	0.8	0.1	0.03	0.1	0.02	0.1	0.06	0.03	0.01	0.10	0.004	0.1	0.1
PG75	3.7	460	N/A	0.06	520	2.67	9.83	2.7	0.60	0.18	0.62	0.09	0.46	0.31	0.32	0.04	0.42	0.004	0.37	0.59
<i>st.dev</i>	0.3	20	N/A	0.01	20	0.05	0.4	0.12	0.03	0.03	0.04	0.01	0.02	0.03	0.04	0.00	0.06	0.002	0.02	0.04
Other objects																				
PG90	2	430	<LOQ	0.06	38	5.0	7.2	4.7	1.0	0.19	0.9	0.12	0.8	0.56	0.45	0.08	3.15	0.024	0.66	1.24
<i>st.dev</i>	1	50	-	0.01	4	0.5	0.5	0.6	0.1	0.01	0.1	0.01	0.1	0.09	0.05	0.01	0.35	0.015	0.08	0.07
PG90y	3	300	<LOQ	0.11	40	6	9	6	1.0	0.25	1.0	0.15	0.9	0.60	0.6	0.08	2.81	0.095	0.9	3.8
<i>st.dev</i>	1	100	-	0.01	20	3	3	2	0.4	0.09	0.5	0.07	0.4	0.24	0.2	0.04	1.20	0.041	0.4	0.2
VG114	7	30	14.57	0.18	50	2.4	5	2.3	0.5	0.12	0.5	0.06	0.4	0.25	0.22	0.03	0.32	0.0001	0.4	1.6
<i>st.dev</i>	2	70	3.63	0.06	10	0.6	1	0.7	0.2	0.04	0.1	0.03	0.1	0.09	0.07	0.01	0.10	0.0001	0.1	0.4

Fig. 4 Comparison of pXRF and LA-ICP-MS data. Binary plots of CaO/SrO vs Fe_2O_3/SrO show that high K_2O glass corresponds to the HMG glass (as determined by LA-ICP-MS) and low K_2O glass corresponds to LMG. The groups are divided by a line to guide the eye. Samples PG2, PG118, PG154, VG52 and VG61 that do not follow the pattern of their groups are marked in the upper plot



would significantly change the discussion about their provenance. For the moment, the only (weak) indication of provenance may be the presence of manganese as a colouring agent, which would link them to an overseas origin of the glass (Koch 2018).

The uniqueness of the high Ba and Ce group of samples can be seen even more clearly in Fig. 6, where they diverge from the general trend formed by the glasses from the Eastern Mediterranean and match well with the aforementioned samples from South Italy discussed in Conte et al. (2019). Samples with flat profiles from both groups align with the Late Bronze Age Mesopotamian glasses discussed by Shortland et al. (2007). Another suggestion that arises from Fig. 6 is that the imported glass was very common in the Italian peninsula during the Iron Age.

This makes most of the HMG group appear unique in the larger context. Without compositionally compatible glass found outside the Italian peninsula, it can be tentatively suggested (until a more complete compositional database arises) that at least part of the samples might be of local origin. Indeed, it would be more feasible to produce plant ash glass in the Italian peninsula, with no historically known high-soda mineral deposits and abundant halophytic plants near the coasts (Sciandrello and Tomaselli 2014). HMG glass production originated in Mesopotamia or Egypt, and the technology may have been somehow transferred to other parts of the Mediterranean (Tait 1991). Interestingly, this technology was used instead of the LMHK glass technology, which flourished in the Italian peninsula during the Final Bronze Age (Henderson 1988; Towle et al. 2001).

Fig. 5 Trace elements values of the analysed samples normalised to the Upper Continental Crust (McLennan 2001): a – for the HMG samples (PG2, 7, 9, 68, 71, 75, 119, 147, VG114); b – for the LMG samples (PG10, 13, 14, 15, 90, 96, 118, 137, 142, 143). External data sources of Iron Age glasses: South Italy – Conte et al. (2019), Central Italy – Yatsuk et al. (2023), Nimrud – Reade (2021), Pieria – Blomme et al. (2017)

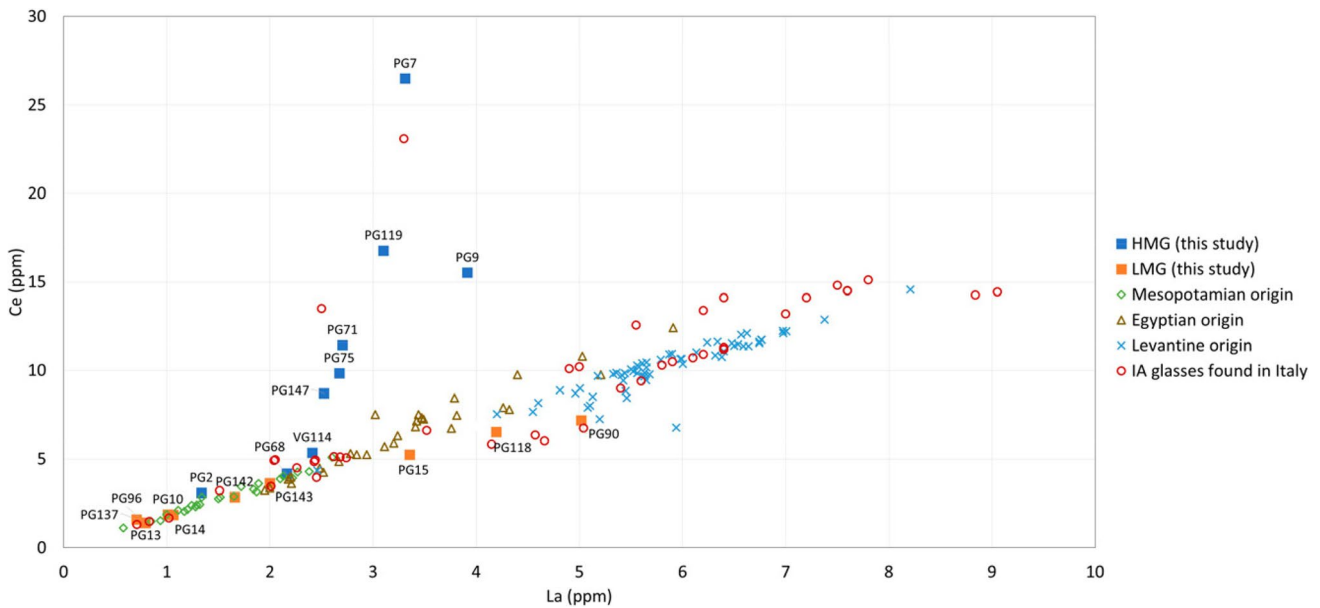
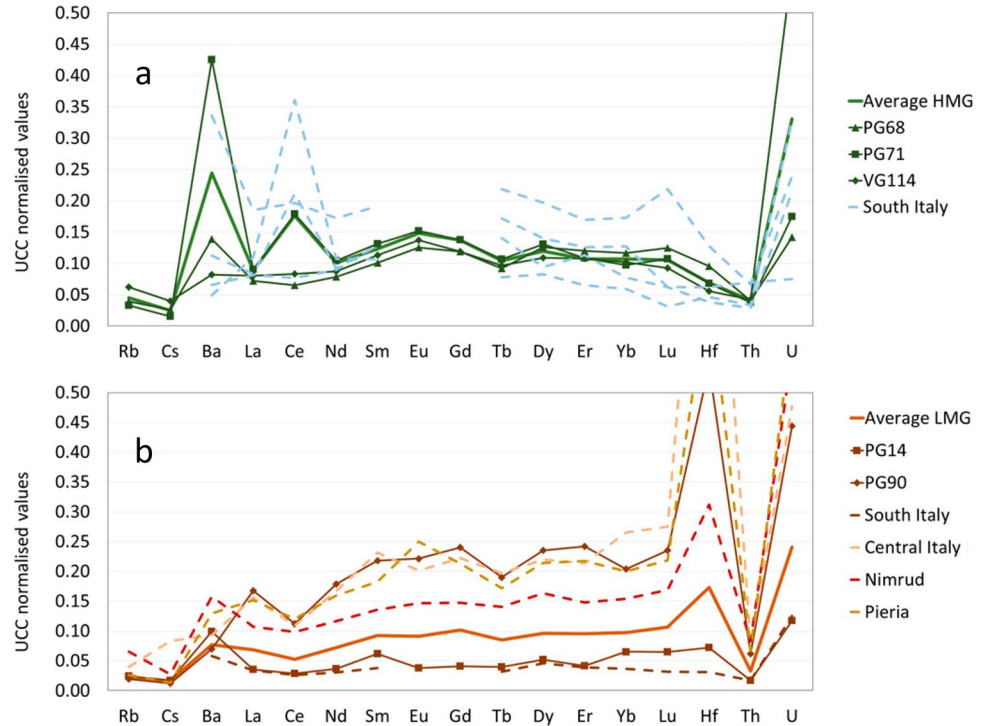


Fig. 6 Binary plot of La against Ce values (LA-ICP-MS data). HMG and LMG samples within this study are compared with glasses of different origin and other Iron Age glasses found in Italian peninsula. External data sources: Mesopotamian and Egyptian origin – Short-

land et al. (2007); Levantine origin – Blomme et al. (2017), Costa et al. (2021); IA glasses found in Italy – Panighello et al. (2012) and Conte (2019)

In any case, the tradition of LMHK glassmaking does not seem to have continued into the Iron Age on the Italian peninsula (Towle et al. 2001; Conte et al. 2019; Yatsuk et al. 2023). Besides the above-discussed samples, the rest of the glasses seem to be imported from Egypt (high Hf LMG)

and Mesopotamia (samples with flat and low trace elements profiles).

Most of the samples in this set owe their colours to the presence of iron, which was likely naturally present in the silica sources (Degryse 2014). The presence of Fe²⁺ and

Fe^{3+} was detected by FORS in the majority of samples that gave meaningful spectra. In addition, several other elements influenced the colours in certain samples. Cu^{2+} was detected in samples PG69 and PG70 during FORS analyses and confirmed by pXRF. This suggests a deliberate addition of copper to colour these beads. VG82 and VG103 (blue oblate beads) contain much lower amount of CuO yet it also influences their colour. The purple coloured PG75 and PG76 show a Mn^{3+} band in the FORS spectrum and contain 0.8 – 1.9% of MnO (determined by pXRF and LA-ICP-MS). Use of manganese for purple colouring has long history in the Mediterranean (Lankton et al. 2022; Muros et al. 2023) and its presence may also be revealed by dark stains on the surface due to glass weathering (Gulmini et al. 2009). Glass of the bulk of the bird beads was coloured by copper (VG88) and by manganese (PG172). Their decorative elements are made of opaque glass, opacified by antimonate containing compounds and coloured by copper (PG172) or both opacified and coloured by lead antimonate (VG88).

Translucent glasses were probably prepared in different ways which is reflected in their apparent colour. For honey-yellow samples, the colour could be created by Fe^{3+} ions in coordination with oxygen or by the formation of ferri-sulphide complex – $\text{Fe}^{3+} - \text{S}^{2-}$ (Schreurs and Brill 1984; Möncke et al. 2014). Strong and broad absorption in the UV-violet part of FORS spectra did not allow to unequivocally confirm the presence of the characteristic band of this chromophore (centred at 405 nm) but there is a reason to assume its presence anyway. In the spectra of honey-yellow samples Fe^{2+} band is usually well-pronounced, even though not so consistently as in other colour groups. Presence of Fe^{2+} should cause the shift of colour to blue, which is not the case. $\text{Fe}^{3+} - \text{S}^{2-}$ is a strong chromophore and can overcome the influence of Fe^{2+} in glass. Formation of ferri-sulphide complex requires reducing conditions (Schreurs and Brill 1984; Meulebroeck et al. 2010), so presence of Fe^{2+} is also expected.

The green and uncoloured glasses are not so different when the colouring mechanism is concerned. These glasses were coloured by iron, particularly Fe^{2+} signal seems to be more consistent in comparison with the honey-yellow group. $\text{Fe}^{2+}/\text{Fe}^{3+}$ ratio must have been managed during the glass production to keep the tinge of the resulting glass in the neutral greenish range (Möncke et al. 2014). In blue samples that are not coloured by copper (PG8, PG9) this ratio must be more in the Fe^{2+} favour than in the rest of the translucent beads.

Noteworthy is the presence of antimony in some of the glasses. With the exception of the PG1, PG8 and PG90, it is present only in the HMG samples. The concentration of the element, almost always less than 1% by weight of oxide, suggests glass decolouring (Silvestri et al. 2008). Interestingly, its presence was detected in many green and uncoloured

glasses, but not so much in the honey-yellow ones. Considering the period to which these glasses are assigned (most are attributed to the eighth century BCE), they could be one of the earliest examples of Sb-decoloured glass ever produced (Biron and Chopinet 2013).

Manganese can also be used to decolour glass. Apart from the purple beads, where it was used in the colouring process, manganese was found in the composition of many high K_2O samples. LA-ICP-MS analysis showed that the MnO content was 0.2% in PG2 and 0.1% in PG71. The MnO concentrations in the samples not analysed in the laboratory are also in this range (Table SI 4). This amount is insufficient to affect the colour of the beads and could be interpreted as an indication of glass recycling, where some Mn-coloured glass was mixed into a new batch of uncoloured glass (Silvestri et al. 2008). At the same time, sands with MnO contents as high as 0.2% have been found on the Italian peninsula (Brems and Degryse 2014). Impurities in the silica source could be the reason for the high MnO content in PG104, as this bead is made of a different type of glass.

Similar (or slightly higher) concentrations of CuO are observed in many high K_2O glasses. However, in the LA-ICP-MS dataset, an elevated CuO amount (up to 200 ppm) is associated with LMG glasses. This may be evidence for recycling in both LMG and HMG glasses.

Another indication of glass recycling is the slightly elevated CoO content (about 40 ppm) in PG9. This amount is several times higher than in other beads, and also seems to be associated with an increased NiO and ZnO amounts, indicating Egyptian alum (Shortland et al. 2006b; Abe et al. 2012). Also, the use of skutterudite, linked to elevated As_2O_3 levels, has been reported in the literature (Genga et al. 2008), and cannot be excluded for this sample. We can therefore assume that some Co-coloured glass entered the batch of PG9. The majority of the examples for which recycling was detected are attributed to the glass that we assumed was locally produced. This means that local artisans used discarded glass to facilitate the melting of the batch and/or to increase the mass of the resulting glass. In any case, they appear to have known how to decolour glass, which is an advanced level of technology for the time.

Conclusion

This study allowed us to collect compositional data for an interesting set of samples, which provided an opportunity to highlight the diverse technological and trade landscape of the Italian peninsula in the eighth-seventh centuries BCE. The compositional analyses of this set of samples, mostly monochrome translucent beads, revealed in fact the diversity of the raw materials that were used for their production. Firstly, several sources of silica were used

as the main component of each batch of glass, suggesting diversified sources of raw glass for the beadmaking. Many samples seem to have been imported from different regions of the Eastern Mediterranean, which is in line with the current view of glass supply in the Iron Age, but it appears that a significant number of the beads considered here were probably produced locally, as evidenced by the uniqueness of the minor and trace element composition. The set of beads and other objects appears to be representative of the two competing traditions in glass making at the time: the use of natron and the plant ash as fluxing agents, which is consistent with the silica sources identified. The imported glass was predominantly produced using a mineral flux (natron), whereas the samples thought to be locally produced were made with plant ash. In addition, the compositional data documented evidence of early glass decolouration and recycling. It is difficult to know where these changes to the primary glass happened. The loose typological classification for the majority of the beads prevents direct parallels, and therefore it is difficult to suggest for them a specific place of production by merging compositional and archaeological evidence. Compositional data may support in the future a more detailed typological classification. Nevertheless, it is important to note that the bird beads and the bowl fragment were attributed to the plant ash glass production, that by the seventh century BCE was on decline in the Mediterranean.

All above said indicates that Southern Etruria and Latium were experiencing the same trends in glass production and supply as the most socially and economically developed parts of the Mediterranean.

Supplementary Information The online version contains supplementary material available at <https://doi.org/10.1007/s12520-024-02038-w>.

Acknowledgements Authors would like to express their gratitude to the administrations of Museo Nazionale Etrusco di Villa Giulia and Museo delle Civiltà for allowing and facilitating the on-site analyses and agreeing to the laboratory study of the objects and to people who handled the collections: Serena Francone, Alessandra Serges and Vittoria Lecce. Acknowledgement is extended to Tiziana Forleo, Vincent Gardette and Pedro Barrulas, who helped in establishing the analytical procedures for micro-Raman and LA-ICP-MS analyses.

Author contributions OY: conceptualisation, validation, formal analysis, investigation, writing—original draft, visualisation, funding acquisition; LK: conceptualisation, investigation, writing – review and editing; LCG: methodology, validation, formal analysis, resources, writing—review and editing; AM: methodology, validation, formal analysis, resources, writing—review and editing; GF: methodology, formal analysis, resources, writing – review and editing; MM: methodology, formal analysis, resources, writing – review and editing; AG: methodology, formal analysis, resources, writing – review and editing; MF: methodology, formal analysis, resources, writing – review and editing; PD: methodology, validation, formal analysis, writing – review and editing; AR: methodology, resources, writing – review and editing; ALG: methodology, resources, writing – review and editing; CI: investigation, writing – review and editing, supervision; MG: methodology,

validation, resources, writing – review and editing, supervision, project administration.

Funding Open access funding provided by Università degli Studi di Torino within the CRUI-CARE Agreement. This project has received funding from the European Union's Horizon 2020 research and innovation program under the Marie Skłodowska-Curie grant agreement No 754511. The contents of this paper are the sole responsibility of the authors and do not necessarily reflect the opinion of the European Union.

Declarations

Competing interest The authors have no competing interests as defined by Springer, or other interests that might be perceived to influence the results and/or discussion reported in this paper.

Open Access This article is licensed under a Creative Commons Attribution 4.0 International License, which permits use, sharing, adaptation, distribution and reproduction in any medium or format, as long as you give appropriate credit to the original author(s) and the source, provide a link to the Creative Commons licence, and indicate if changes were made. The images or other third party material in this article are included in the article's Creative Commons licence, unless indicated otherwise in a credit line to the material. If material is not included in the article's Creative Commons licence and your intended use is not permitted by statutory regulation or exceeds the permitted use, you will need to obtain permission directly from the copyright holder. To view a copy of this licence, visit <http://creativecommons.org/licenses/by/4.0/>.

References

- Abd-Allah R (2022) From Decolorization to Solarization of Historical Glass: A review. *Advanced Research in Conservation Science* 3:30–41. <https://doi.org/10.21608/args.2022.135911.1025>
- Abe Y, Harimoto R, Kikugawa T et al (2012) Transition in the use of cobalt-blue colorant in the New Kingdom of Egypt. *J Archaeol Sci* 39:1793–1808. <https://doi.org/10.1016/j.jas.2012.01.021>
- Angelini I, Gratuze B, Artioli G (2019) Glass and other vitreous materials through history. In: *The Contribution of Mineralogy to Cultural Heritage*. Mineralogical Society of Great Britain and Ireland. 87–150
- Babbi A (2003) I reperti della necropoli delle Arcatelle di Tarquinia al Museo L. Pigorini *Bullettino Di Paletnologia Italiana* 93–94:115–154
- Bietti Sestieri AM (1992) *La necropoli laziale di Osteria dell'Osa*. Quasar, Roma
- Biron I, Chopinet M (2013) Colouring, Decolouring and Opacifying of Glass. In: Janssens K (ed) *Modern Methods for Analysing Archaeological and Historical Glass*, 1st edn. Wiley, pp 49–65
- Blomme A, Degryse P, Dotsika E et al (2017) Provenance of polychrome and colourless 8th–4th century BC glass from Pieria, Greece: A chemical and isotopic approach. *J Archaeol Sci* 78:134–146. <https://doi.org/10.1016/j.jas.2016.12.003>
- Brems D, Degryse P (2014) Trace elements in sand raw materials. In: Degryse P (ed) *Glass Making in the Greco-Roman World: Results of the ARCHGLASS project*. Leuven University Press, Leuven, Belgium, pp 69–86
- Brill RH (1963) Ancient Glass. *Sci Am* 209:120–131
- Brusadin Laplace D, Patrizi-Montoro G, Patrizi-Montoro S (1992) Le necropoli protostoriche del Sasso di Furbara III. Caolino e altri sepolcreti villanoviani. In: *Origini*. 221–294

- Carlucci C, De Lucia MA (1998) Villa Giulia Museum: the antiquities of the Faliscans. "L'Erma" di Bretschneider: Ingegneria per la cultura, Roma
- Cellerino A (2021) Transparent glass drinking bowls at the assyrian court: visual appeal of wine consumption. *Mesopotamia: rivista di archeologia, epigrafia e storia orientale antica*: LVI, 2021. <https://doi.org/10.1400/290952>
- Conte S, Arletti R, Henderson J et al (2018) Different glassmaking technologies in the production of Iron Age black glass from Italy and Slovakia. *Archaeol Anthropol Sci* 10:503–521. <https://doi.org/10.1007/s12520-016-0366-4>
- Conte S, Matarese I, Vezzalini G et al (2019) How much is known about glassy materials in Bronze and Iron Age Italy? New data and general overview. *Archaeol Anthropol Sci* 11:1813–1841. <https://doi.org/10.1007/s12520-018-0634-6>
- Conte S, Arletti R, Mermati F, Gratuze B (2016) Unravelling the Iron Age glass trade in southern Italy: the first trace-element analyses. *ejm* 28:409–433. <https://doi.org/10.1127/ejm/2016/0028-2516>
- Costa M, Barrulas P, Arruda AM et al (2021) An insight into the provenance of the Phoenician-Punic glass beads of the necropolis of Vinha das Calças (Beja, Portugal). *Archaeol Anthropol Sci* 13:149. <https://doi.org/10.1007/s12520-021-01390-5>
- Degryse P (ed) (2014) Glass making in the Greco-Roman world: results of the ARCHGLASS project. Leuven University Press, Leuven, Belgium
- Delpino F (1977) La prima età del ferro a Bisenzio, divisione in fasi ed interpretazione culturale. (Le I Age du Fer à B., subdivisions chronologiques et interprétation culturelle). *Studi Etruschi* 45:39–49
- Falconi Amorelli MT, Close-Brooks J, De Agostino A, et al (1963) Veio - Isola Farnese. Scavi di una necropoli villanoviana in località „Quattro Fontanili”, *Accademia degli Lincei*. Roma
- Ferri LD, Mezzadri F, Falcone R et al (2020) A non-destructive approach for the characterization of glass artifacts: The case of glass beads from the Iron Age Picene necropolises of Novilara and Crocefisso-Matelica (Italy). *J Archaeol Sci Rep* 29:102124. <https://doi.org/10.1016/j.jasrep.2019.102124>
- Genga A, Siciliano M, Tepore A et al (2008) An archaeometric approach about the study of medieval glass from Siponto (Foggia, Italy). *Microchem J* 90:56–62. <https://doi.org/10.1016/j.microc.2008.03.008>
- Gulmini M, Pace M, Ivaldi G et al (2009) Morphological and chemical characterization of weathering products on buried Sasanian glass from central Iraq. *J Non-Cryst Solids* 355:1613–1621. <https://doi.org/10.1016/j.jnoncrsol.2009.05.056>
- Henderson J (1985) The Raw Materials of Early Glass Production. *Oxford J Archaeology* 4:267–291. <https://doi.org/10.1111/j.1468-0092.1985.tb00248.x>
- Henderson J (1988) Electron Probe Microanalysis of Mixed-Alkali Glasses. *Archaeometry* 30:77–91. <https://doi.org/10.1111/j.1475-4754.1988.tb00436.x>
- Henderson J (2013) *Ancient Glass: An Interdisciplinary Exploration*, 1st edn. Cambridge University Press
- Ignatiadou D (2012) Early Glass in Methone. In: Lazar I (ed) *Annales du 19e Congrès de l'Association Internationale pour l'Histoire du Verre*. Koper, Piran. 81–88
- Kaparou M, Oikonomou A (2022) Mycenaean through Hellenistic glass in Greece: where have we got to? *Archaeol Anthropol Sci* 14:92. <https://doi.org/10.1007/s12520-022-01558-7>
- Koch LC (2018) Report on the Vitreous Bird Beads (Vogelperlen). *Arimnestos: Ricerche Di Protostoria Mediterranea* 1:227–237
- Koch LC (2020) An Overview of Vitreous Materials in Bronze Age Italy and Brief Perspectives on the Iron Age. In: Pernicka E, Rose CB, Jablonka P (eds) *From Past to Present. Studies in Memory of Manfred O. Korfmann*, Verlag Dr. Rudolf Habelt GMBH. Bonn. 409–426
- Kolesnychenko A, Kiosak D (2018) The Ancient Glass-Workshop of Yahorlyk Settlement in the Northern Pontic Region. In: *Annales du 21e Congrès de l'AIHV Istanbul 2018* O. Sevindik Ed. Pavia: 2021;81–94. In: Sevindik O (ed) *Annales du 21e Congrès de l'AIHV*. Pavia, Istanbul. 81–94
- Lahlil S, Cotte M, Biron I et al (2011) Synthesizing lead antimonate in ancient and modern opaque glass. *J Anal At Spectrom* 26:1040. <https://doi.org/10.1039/c0ja00251h>
- Lankton JW, Pulak C, Gratuze B (2022) Glass ingots from the Uluburun shipwreck: Glass by the batch in the Late Bronze Age. *J Archaeol Sci Rep* 42:103354. <https://doi.org/10.1016/j.jasrep.2022.103354>
- Ligabue G (2022) *Falerii Veteres: il sepolcreto di Montarano scavi, materiali e contesti*. Giorgio Bretschneider editore, Roma
- McLennan SM (2001) Relationships between the trace element composition of sedimentary rocks and upper continental crust: Trace element composition and upper continental crust. *Geochem Geophys Geosyst* 2:n/a-n/a. <https://doi.org/10.1029/2000GC000109>
- Mengarelli L, Savignoni R (1903) Caracupa: la necropoli arcaica di Caracupa tra Norba e Sermoneta. In: *Atti della R. Accademia dei Lincei. Memorie della Classe di scienze morali, storiche e filologiche*, Accademia dei Lincei. Rome. 289–344
- Meulebroeck W, Baert K, Wouters H, et al (2010) The identification of chromophores in ancient glass by the use of UV-VIS-NIR spectroscopy. In: Berghmans F, Mignani AG, Van Hoof CA (eds). Brussels, Belgium. 77260D
- Micheletti F, Orsilli J, Melada J et al (2020) The role of IRT in the archaeometric study of ancient glass through XRF and FORS. *Microchem J* 153:104388. <https://doi.org/10.1016/j.microc.2019.104388>
- Mildner S, Schüssler U, Falkenstein F, Brätz H (2018) Bronzezeitliches "High Magnesium Glass" in Mitteleuropa – Lithium und Bor als Indizien für eine mögliche Herkunft aus Westanatolien. In: Glaser L (ed) *Archäometrie und Denkmalpflege*. Hamburg. 132–135
- Mirti P, Davit P, Gulmini M (2002) Colourants and opacifiers in seventh and eighth century glass investigated by spectroscopic techniques. *Anal Bioanal Chem* 372:221–229. <https://doi.org/10.1007/s00216-001-1183-9>
- Mirti P, Pace M, Negro Ponzi MM, Aceto M (2008) ICP-MS analysis of glass fragments of Parthian and Sasanian epoch from Seleucia and Veh Ardašir (Central Iraq). *Archaeometry* 50:429–450. <https://doi.org/10.1111/j.1475-4754.2007.00344.x>
- Möncke D, Papageorgiou M, Winterstein-Beckmann A, Zacharias N (2014) Roman glasses coloured by dissolved transition metal ions: redox-reactions, optical spectroscopy and ligand field theory. *J Archaeol Sci* 46:23–36. <https://doi.org/10.1016/j.jas.2014.03.007>
- Moretti C, Hreglich S (2013) Raw Materials, Recipes and Procedures Used for Glass Making. In: Janssens K (ed) *Modern Methods for Analysing Archaeological and Historical Glass*, 1st edn. Wiley, pp 23–47
- Muros V, Zacharias N, Henderson J (2023) The composition and provenance of Late Bronze Age vitreous materials from Kefalonia. *Greece Journal of Archaeological Science: Reports* 51:104218. <https://doi.org/10.1016/j.jasrep.2023.104218>
- O'hea M, (2011) Another Look at the Origins of Iron Age II Cast Glass Vessels in the Levant. *Levant* 43:153–172. <https://doi.org/10.1179/175638011X13112549593023>
- Oikonomou A, Triantafyllidis P (2018) An archaeometric study of Archaic glass from Rhodes, Greece: Technological and provenance issues. *J Archaeol Sci Rep* 22:493–505. <https://doi.org/10.1016/j.jasrep.2018.08.004>
- Olmeda G (2015) Evolution of ornamental vitreous materials in Italy from the Middle Bronze Age to the Iron Age: case studies from Lipari and from the Veneto region. University of Padua

- Palm J (1952) Veiiian Tomb Groups in the Museo Preistorico. In: *Opuscula Archaeologica*, Gleerup. Lund. 50–86
- Panighello S, Orsega EF, van Elteren JT, Šelih VS (2012) Analysis of polychrome Iron Age glass vessels from Mediterranean I, II and III groups by LA-ICP-MS. *J Archaeol Sci* 39:2945–2955. <https://doi.org/10.1016/j.jas.2012.04.043>
- Paribeni R (1906) Necropoli del territorio capenate. *Monumenti Antichi Dei Lincei* 16:277–490
- Purowski T, Dzierżanowski P, Bulska E et al (2012) A study of glass beads from the Hallstatt C-D from southwestern Poland: implications for glass technology and provenance. *Archaeometry* 54:144–166. <https://doi.org/10.1111/j.1475-4754.2011.00619.x>
- Purowski T, Kępa L, Wagner B (2018) Glass on the Amber Road: the chemical composition of glass beads from the Bronze Age in Poland. *Archaeol Anthropol Sci* 10:1283–1302. <https://doi.org/10.1007/s12520-016-0443-8>
- Reade W (2021) The first thousand years of glass-making in the ancient Near East: compositional analyses of late Bronze and Iron Age glasses. Archaeopress Publishing Ltd, Oxford
- Reade W, Freestone IC, Bourke S (2006) Innovation and continuity in bronze and iron age glass from Pella In Jordan. 9
- Reade W, Jones JD, Privat K (2009) Iron Age and Hellenistic monochrome glasses from Gordion. In: *Annales du 18e Congrès AIHV. Thessaloniki*. 87–93
- Rehren Th (2000) Rationales in Old World Base Glass Compositions. *J Archaeol Sci* 27:1225–1234. <https://doi.org/10.1006/jasc.1999.0620>
- Rehren Th (2008) A review of factors affecting the composition of early Egyptian glasses and faience: alkali and alkali earth oxides. *J Archaeol Sci* 35:1345–1354. <https://doi.org/10.1016/j.jas.2007.09.005>
- Rehren Th, Freestone IC (2015) Ancient glass: from kaleidoscope to crystal ball. *J Archaeol Sci* 56:233–241. <https://doi.org/10.1016/j.jas.2015.02.021>
- Sayre EV, Smith RW (1961) Compositional Categories of Ancient Glass. *Science* 133:1824–1826. <https://doi.org/10.1126/science.133.3467.1824>
- Schreurs JWH, Brill RH (1984) Iron and sulfur related colors in ancient glasses. *Archaeometry* 26:199–209. <https://doi.org/10.1111/j.1475-4754.1984.tb00334.x>
- Sciandrello S, Tomaselli V (2014) Coastal salt-marshes plant communities of the Salicornietea fruticosae class in Apulia (Italy). *Biologia* 69:53–69. <https://doi.org/10.2478/s11756-013-0283-2>
- Sgubini Moretti AM (2001) Veio, Cerveteri, Vulci. Città d'Etruria a Confronto. Roma, Museo Nazionale Etrusco Di Villa Giulia. Villa Poniatowski. 2001, 1 Ottobre-30 Dicembre. L'Erma di Bretschneider, Roma
- Shortland A, Schachner L, Freestone I, Tite M (2006a) Natron as a flux in the early vitreous materials industry: sources, beginnings and reasons for decline. *J Archaeol Sci* 33:521–530. <https://doi.org/10.1016/j.jas.2005.09.011>
- Shortland AJ, Tite MS, Ewart I (2006b) Ancient exploitation and use of cobalt alums from the western oases of Egypt. *Archaeometry* 48:153–168. <https://doi.org/10.1111/j.1475-4754.2006.00248.x>
- Shortland A, Rogers N, Eremin K (2007) Trace element discriminants between Egyptian and Mesopotamian Late Bronze Age glasses. *J Archaeol Sci* 34:781–789. <https://doi.org/10.1016/j.jas.2006.08.004>
- Silvestri A, Molin G, Salviulo G (2008) The colourless glass of Iulia Felix. *J Archaeol Sci* 35:331–341. <https://doi.org/10.1016/j.jas.2007.03.010>
- Solé VA, Papillon E, Cotte M et al (2007) A multiplatform code for the analysis of energy-dispersive X-ray fluorescence spectra. *Spectrochim Acta, Part B* 62:63–68. <https://doi.org/10.1016/j.sab.2006.12.002>
- Stefanì E (1912) Scoperte archeologiche nell'Agro Capenate. In: *Bollettino di Paleontologia Italiana*. 147–158
- Tait H (1991) Five thousand years of glass. British museum press, London
- Taloni M (2013) Le tombe da Riserva del Truglio al museo Pigorini di Roma. Officina edizioni, Roma
- Tite MS, Shortland A, Maniatis Y et al (2006) The composition of the soda-rich and mixed alkali plant ashes used in the production of glass. *J Archaeol Sci* 33:1284–1292. <https://doi.org/10.1016/j.jas.2006.01.004>
- Towle A, Henderson J, Bellintani P, Gambacurta G (2001) Frattesina and Adria: report of scientific analyses of early glass from the Veneto. In: Fabrizio S (ed) Padusa. Pisa. 1–62
- Wedepohl KH, Simon K, Kronz A (2011) Data on 61 chemical elements for the characterization of three major glass compositions in Late Antiquity and the Middle Ages. *Archaeometry* 53:81–102. <https://doi.org/10.1111/j.1475-4754.2010.00536.x>
- Yatsuk O, Ferretti M, Gorghinian A et al (2022) Data from Multiple Portable XRF Units and Their Significance for Ancient Glass Studies. *Molecules* 27:6068. <https://doi.org/10.3390/molecules27186068>
- Yatsuk O, Koch L, Gorghinian A et al (2023) An archaeometric contribution to the interpretation of blue-green glass beads from Iron age Central Italy. *Herit Sci* 11:113. <https://doi.org/10.1186/s40494-023-00952-1>

Publisher's Note Springer Nature remains neutral with regard to jurisdictional claims in published maps and institutional affiliations.